

Chandra Observations of the Interacting NGC 4410 Galaxy Group

Beverly J. Smith

*Department of Physics and Astronomy, East Tennessee State University, Johnson City TN
37614*

smithbj@etsu.edu

Michael Nowak

Massachusetts Institute of Technology

mnowak@alum.mit.edu

Megan Donahue

Space Telescope Science Institute

donahue@stsci.edu

and

John Stocke

CASA, University of Colorado

stocke@casa.colorado.edu

ABSTRACT

We present high resolution X-ray imaging data from the ACIS-S instrument on the Chandra telescope of the nearby interacting galaxy group NGC 4410. Four galaxies in the inner portion of this group are clearly detected by Chandra, including the peculiar low luminosity radio galaxy NGC 4410A. In addition to a nuclear point source, NGC 4410A contains diffuse X-ray emission, including an X-ray ridge extending out to about $12''$ (6 kpc) to the northwest of the nucleus. This ridge is coincident with an arc of optical emission-line gas, which has previously been shown to have optical line ratios consistent with shock ionization. This structure may be due to an expanding superbubble of hot gas caused by supernovae and stellar winds or by the active nucleus. The Chandra observations

also show four or five possible compact ultra-luminous X-ray (ULX) sources ($L_x \geq 10^{39}$ erg s $^{-1}$) associated with NGC 4410A. At least one of these candidate ULXs appears to have a radio counterpart, suggesting that it may be due to an X-ray binary with a stellar-mass black hole, rather than an intermediate mass black hole. In addition, a faint diffuse intragroup X-ray component has been detected between the galaxies ($L_x \sim 10^{41}$ erg s $^{-1}$). This supports the hypothesis that the NGC 4410 group is in the process of evolving via mergers from a spiral-dominated group (which typically have no X-ray-emitting intragroup gas) to an elliptical-dominated group (which often have a substantial intragroup medium).

Subject headings: Galaxies: Active—Galaxies: Individual: NGC Number: NGC 4410—X-Rays: Galaxies

1. Introduction

There has been increasing evidence in recent years that most elliptical galaxies are the result of the merging of disk galaxies (e.g., Barnes (1985); Barnes & Hernquist (1992)). The optical counterparts of luminous radio galaxies are generally elliptical or elliptical-like galaxies (Owen & White 1991), which suggests that the creation of radio jets may somehow be linked to the merger process (Wilson et al. 1995; Moderski & Sikora 1996). Once a radio jet is formed, its subsequent evolution may be affected by further galaxy interactions and mergers. For example, it may be distorted by motion through an intracluster medium (Miley et al. 1972), by an encounter with interstellar matter in either a host galaxy (De Young 1981) or a companion galaxy (Stocke et al. 1985; Borne & Colina 1993) or by a galaxy in the process of merging with the host galaxy (Van Breugel et al. 1986). In addition, impacts between jets and interstellar matter may trigger star formation in some cases (De Young 1981; Van Breugel et al. 1985).

It is difficult to study these processes because most elliptical galaxies, and most radio galaxies, reside in rich clusters where the merger events took place very long ago. Some ellipticals, however, are found in poor groups in the current epoch (see, e.g., Mulchaey & Zabludoff (1998)), which are only now undergoing the merger events that took place long ago in rich clusters. Poor, compact groups of galaxies, therefore, are the locations best suited for investigating the merger process. Mulchaey & Zabludoff (1998) have found hot, X-ray halos around dominant ellipticals in poor galaxy groups, however, usually the elliptical already looks completely formed and the gaseous halo is relaxed. Evidently, the actual merger events themselves happen so quickly that there are very few nearby examples. If a few examples were found, however, they would offer a complex set of observational constraints

since the merging participants could include gas and stars from a remnant disk galaxy, new star formation driven by the merger, inception of AGN activity in one or more nuclei, and jet driven formation by the newly created radio jet. We have discovered a nearby example of a likely merger in progress: NGC 4410.

The NGC 4410 group contains about a dozen members, with five major galaxies in its inner portions, at least four of which appear to be strongly interacting (see Figure 1). This group is quite nearby (97 Mpc, for $H_0 = 75 \text{ km s}^{-1} \text{ Mpc}^{-1}$), and is well-studied at radio and optical wavelengths (Hummel et al. 1986; Smith 2000; Donahue et al. 2002). The four brightest galaxies in the inner group and the four brightest in the outer group are classified as spiral or S0 galaxies in the NASA/IPAC Extragalactic Database (NED¹). The most luminous member at optical wavelengths, NGC 4410A, classified as an Sab? peculiar galaxy by de Vaucouleurs et al. (1993), is a low luminosity radio galaxy with a very distorted double-lobed radio morphology (Hummel et al. 1986; Smith 2000). The peculiar radio structure strongly suggests that the radio jet has been affected by motion relative to interstellar or intracluster gas (Stocke & Burns 1987; Smith 2000). NGC 4410A has a peculiar ring-like optical morphology, with six extremely luminous H II regions ($L_{H\alpha} = 10^{40}\text{--}10^{41} \text{ erg sec}^{-1}$) lying along this structure (Figure 2; (Donahue et al. 2002)). At present, it is not clear whether the star formation in NGC 4410A was triggered by pressure from the radio lobes on the ambient medium, or by a gravitational interaction or collision with NGC 4410B. The western portion of this ring has optical line ratios consistent with shock ionization (Donahue et al. 2002). NGC 4410A has been detected in both 21 cm H I and 2.6mm CO ($M_{\text{HI}} = 1.3 \times 10^9 M_{\odot}$ and $M_{\text{H}_2} = 3.9 \times 10^9 M_{\odot}$, assuming the standard Galactic conversion factor) (Smith 2000). A prominent H I tail has been discovered, aligned along a stellar tail extending 1.7 arcmin (50 kpc) to the southeast of the NGC 4410A/NGC 4410B pair (Smith 2000). Both the radio galaxy NGC 4410A and its nearby companion NGC 4410B are classified as Low Ionization Nuclear Emission Region (LINER) galaxies (Mazzarella & Boroson 1993; Donahue et al. 2002), and NGC 4410D and F also show optical emission lines (Stocke & Burns 1987).

Clues to the history of the NGC 4410 system may come from X-ray data. The NGC 4410A group has previously been mapped in X-rays with both the High Resolution Imager (HRI) and the Position Sensitive Proportional Counter (PSPC) instruments on ROSAT (Tschöke et al. 1999; Smith 2000). The global PSPC spectrum has been deconvolved into two components: a power-law spectrum, contributing 2/3 of the X-ray radiation, and a 1 keV thermal component, contributing the remaining light (Tschöke et al. 1999). The

¹The NASA/IPAC Extragalactic Database at <http://nedwww.ipac.caltech.edu> is operated by the Jet Propulsion Laboratory, California Institute of Technology, under contract with the National Aeronautics and Space Administration

HRI map shows a point source associated with the nucleus of NGC 4410A and a diffuse halo extending $10''$ to the southeast, towards the most luminous H II region. The halo contributes approximately $1/3$ of the total light in the HRI map, supporting its association with the thermal component in the PSPC spectral decomposition. The lower resolution PSPC map shows a faint tail-like feature extending eastwards from the NGC 4410A+B pair towards NGC 4410C, anti-coincident with the southeastern H I tail. From the ROSAT data, it was not clear whether this X-ray emission is due to shocked gas in the tidal bridge, as has been suggested for X-ray-emitting gas associated with a tidal tail in the radio galaxy Fornax A (Mackie & Fabbiano 1998), intragroup gas that is coincidentally superposed on the stellar bridge, or simply background or foreground sources.

2. Observations

To address these issues, we have made higher resolution X-ray observations of the NGC 4410 galaxy group in imaging mode with the backside-illuminated Advanced CCD Imaging Spectrometer (ACIS) S3 chip on the Chandra X-ray telescope (Weisskopf et al. 2002). The nucleus of NGC 4410A was placed near the nominal aimpoint of this chip, and the roll angle during the observations was 203° west of north. The ACIS chips have 1024×1024 $0''.492$ pixels. To reduce pile-up, we only read out 640 chip rows, giving an observed field of view of $5'.2 \times 8'.4$. The other four galaxies in the inner group (NGC 4410B, C, D, and F) also fell on this chip. The CCD temperature was -120° C, the frame time was 2.1 seconds, and the events were telemetered in Faint mode. In addition to the S3 chip (the main focus of this paper), the S1, S2, S4, I3, and I4 chips of ACIS were also read out.

Initial data reductions were done using the CIAO v2.2.1 software². After removing time intervals with high X-ray background, the useable exposure time was 34.3 ksec. Only events with ASCA grades 0, 2, 3, 4, and 6 were included, and standard bad pixels and columns were removed. The energy range was restricted to $0.3 - 8$ keV, and then further divided into three ranges: $0.3 - 1$ keV, $1 - 2.5$ keV, and $2.5 - 8$ keV. The binned images were adaptively smoothed using the CIAO routine `csmooth`, using a minimal significance of $S/N = 2.5$ and a maximal significance of $S/N = 5$. The smoothed images were then divided by a similarly-smoothed exposure map to convert into physical units and to remove instrumental artifacts. We experimented with exposure maps created using different parameters, including both monochromatic maps at various energies and weighted maps. In all cases, the basic

²CIAO is the Chandra Interactive Analysis of Observations data analysis system package (<http://exc.harvard.edu/ciao>)

morphology of the extended emission in the group remained the same, although the absolute flux level varied. For our final 0.3 – 8 keV map, we used an exposure map weighted by the spectrum of a $57''.5 \times 40''$ region centered on the NGC 4410A+B complex. For the final 0.3 – 1 keV, 1 – 2.5 keV, and 2.5 – 8 keV maps, we used monochromatic 0.8 keV, 1.5 keV, and 3 keV exposure maps, respectively.

3. Results

3.1. Morphology

In Figure 3, we provide the final 0.3 – 8 keV ACIS-S S3 Chandra map (greyscale), with optical contours from the Digitized Sky Survey³ (DSS) superposed. This figure shows that four galaxies in the inner part of the NGC 4410 group were detected by Chandra: NGC 4410A+B, NGC 4410C, and NGC 4410D. Several point sources are also visible in this map, including two sources in the NGC 4410A+B–C bridge. The more northeastern of these sources (at $12^{\text{h}} 26^{\text{m}} 33.5^{\text{s}}$, $9^{\circ} 1' 45''$ (J2000)), is particularly bright, with a total of 175 0.3 – 8 keV counts, and is slightly extended ($\sim 2'' \times 3''$).

This map also shows faint extended emission in the group, concentrated around NGC 4410A+B, and extending out past NGC 4410C. Over the mapped portion of the group, for the diffuse X-ray emission outside of the main optical galaxies, the average Chandra 0.3 – 8 keV counts are $9 \pm 2 \times 10^{-10}$ photons $\text{s}^{-1} \text{cm}^{-2} \text{pixel}^{-1}$, with the uncertainty dominated by the uncertainty in the exposure map (the statistical noise is only $\sim 0.3 \times 10^{-10}$ photons $\text{s}^{-1} \text{cm}^{-2} \text{pixel}^{-1}$). Assuming a typical energy per photon of 0.8 keV, this corresponds to $5 \pm 1 \times 10^{-18}$ erg $\text{s}^{-1} \text{cm}^{-2} \text{arcsec}^{-2}$, consistent with the upper limit from the ROSAT data (Smith 2000).

Another concentration of extended emission is visible to the northeast of NGC 4410D, at $\sim 12^{\text{h}} 26^{\text{m}} 47^{\text{s}}$, $9^{\circ} 4' 15''$. This region of X-ray emission is also present in the ROSAT maps of Tschöke et al. (1999). In the higher resolution Chandra map, it is resolved into four point sources, surrounded by extended emission. One of these X-ray sources has a possible optical counterpart in the DSS image. These point sources may be background QSOs or

³The Digitized Sky Survey was produced at the Space Telescope Science Institute under U.S. Government grant NAG W-2166. These images are digitized versions of photographic plates from the Second Palomar Observatory Sky Survey (POSS-II) made by the California Institute of Technology with funds from the National Science Foundation, the National Geographic Society, the Sloan Foundation, the Samuel Oshin Foundation, and the Eastman Kodak Corporation

radio galaxies in a distant cluster rich in hot X-ray-emitting intracluster gas.

In Figure 4, the low energy (0.3 – 1 keV) map is presented, again superposed on the DSS image. The extended emission in this map has a morphology similar to that in the total 0.3 – 8 keV map. Extended emission is visible around NGC 4410A+B extending up to NGC 4410C. The second concentration to the northeast of NGC 4410D is also visible. In this low energy map, a faint source is visible near NGC 4410F.

In the middle energy (1 – 2.5 keV) map (Figure 5), the morphology of the central region is similar to that seen in the low energy map. In the northeast, however, the morphology is somewhat different. In particular, the point source northeast of NGC 4410D with the possible optical counterpart is no longer visible.

At even higher energies (2.5 – 8 keV; Figure 6), the nucleus of NGC 4410A is quite bright, as is the more northeastern point source in the NGC 4410A+B-C bridge. NGC 4410C and D, however, are quite faint, and NGC 4410F is undetected. This map shows a different extended morphology in the central regions than the lower energy maps, although we note that the highest energies are the most likely to be contaminated by background. Faint diffuse emission is visible between NGC 4410A+B and C, and north of NGC 4410D. If this is real, it implies that the intracluster gas in this region is hotter than in the rest of the group.

The Chandra position of the nucleus of NGC 4410A agrees with the radio continuum peak position from Hummel et al. (1986) within 0.1". The 4.9 GHz radio continuum map of the NGC 4410 group from Hummel et al. (1986) is superposed on the 0.3 – 8 keV Chandra map in Figure 7. Note the apparent anti-coincidence of the extended X-ray and radio emission in the southeast. The radio continuum lobe lies to the south, while the X-ray emission extends approximately east-west. The Chandra field of view does not extend beyond the radio lobe, so it is not known whether the radio lobe is surrounded by X-ray-emitting gas. The northern radio lobe, seen in the lower resolution map of Smith (2000), is too faint to be visible in this higher resolution Hummel et al. (1986) map.

An expanded view of the portion of the 0.3 – 8 keV map around NGC 4410A+B is shown in Figure 8, and, in Figure 9, a red archival Hubble Space Telescope image is superposed as contours on the unsmoothed Chandra map. In Figure 10, the Donahue et al. (2002) H α + [N II] map is superposed on the Chandra map. The bright X-ray peak is associated with the NGC 4410A nucleus, while the secondary source to the east is coincident with the NGC 4410B nucleus. A ridge of X-ray emission extending $\sim 12''$ (6 kpc) to the northwest of NGC 4410A is also visible, coincident with the ionized gas in the northwestern portion of the optical loop (Figure 10). As noted earlier, this gas has optical line ratios indicative of

shock ionization (Donahue et al. 2002). Note that the $3''$ extension to the southwest of the NGC 4410A nucleus seen in the optical line map is also present in X-rays. Note also that the optically-bright knots to the southeast and northeast of the nucleus of NGC 4410A are not visible as discrete sources in the X-ray map. These sources are known to be luminous H II regions (Donahue et al. 2002).

3.2. X-Ray Spectra

Spectra of NGC 4410A – D, the brightest bridge source in the NGC 4410A+B–C bridge, and the diffuse intragroup gas were extracted from the data using CIAO, and spectral analysis was accomplished using the ISIS data reduction package (Houck & Denicola 2000). Results of spectral fitting are given in Table 1 and Figures 11 and 12. Unless otherwise noted, the $0.5 - 5$ keV range was used for fitting the spectra, eliminating the low S/N high energy portion plus the lower energies where the calibration is somewhat uncertain. The quoted uncertainties are 90% confidence level. Before fitting the spectra, the data were rebinned into 20 counts bin^{-1} and the recent CIAO *apply_acisabs* correction for contamination of the ACIS chips was applied. To estimate background counts, the deep ACIS observations of blank fields provided by M. Markevitch were used (file *acis7sD2000-12-01bkgrndN0002.fits*).

In no case were we able to successfully constrain the absorption column, the normalization, and the power law index or temperature simultaneously. For NGC 4410A, we divided the source into three radial regimes: $< 1''$, $1'' - 5''$, and $5'' - 10''$. The nucleus of NGC 4410A is relatively bright (1256 counts in a 4.25 pixel radius), so we also included the effects of pile-up for the central region. When fixing the absorption to a nominal value of $5 \times 10^{20} \text{ cm}^{-2}$ (approximately equal to the sum of the $1.7 \times 10^{20} \text{ cm}^{-2}$ Galactic absorption from Dickey & Lockman (1990) and the intrinsic HI column densities from Smith (2000)), for the inner $1''$ we obtained an adequate fit to a power law with photon index $\Gamma \sim 2$ (see Table 1). Conversely, by fixing the photon index to this value, we obtained column densities consistent with the nominal value. Increasing the photon index increases the fitted column density, still providing good fits with reasonable column density up to $\Gamma \sim 2.3$. Models without pile-up give similar results.

For the $1'' - 5''$ and $5'' - 10''$ annuli around NGC 4410A, the spectra can be fit with Mekal functions, with temperatures $kT = 0.62 \pm_{0.07}^{0.08} \text{ keV}$ and $0.54 \pm_{0.14}^{0.12} \text{ keV}$ and abundances of $0.06 \pm_{0.03}^{0.06}$ and $0.11 \pm_{0.09}^{1.16}$ solar, respectively. For fitting the inner and outer annuli, we only included photons with energies $0.6 - 1.8 \text{ keV}$ and $0.6 - 1.2 \text{ keV}$; at higher energies, the counts are consistent with the background.

The nuclei of B, C, and D had very few counts, so it was not possible to do detailed fitting of their spectral shapes. For these objects, we fixed both the absorbing column and the spectral parameters, and checked for consistency. All three spectra are consistent with bremsstrahlung spectra, and are consistent with both the Galactic absorption alone or with the nominal internal absorption included. The NGC 4410B spectrum appears relatively soft, consistent with a $kT = 0.2$ keV temperature, while NGC 4410C and D are consistent with $kT = 0.5 - 1$ keV.

For the bridge source (named ‘b1’ in Table 1), we found a good fit to the photon index $\Gamma = 2.2 \pm 0.3$ with the nominal extinction. If it is at the distance of NGC 4410, it has a luminosity of 4×10^{40} erg s $^{-1}$. At that distance, the angular extent of the source corresponds to a size of ~ 1 kpc \times 1.5 kpc.

To obtain the spectrum and luminosity of the diffuse intragroup medium, we extracted counts in a $6'.4 \times 4'.6$ (180×130 kpc) diameter ellipse aligned east-west, centered at $12^h 26^m 32.7^s$, $9^\circ 1' 45''.5$ (J2000), excluding $51''$, $21''$, and $21''$ diameter circular regions around NGC 4410A+B, NGC 4410C, and NGC 4410D, respectively, as well as $5''$ radius regions around the bright bridge source and 11 point sources visible in the field (including the point sources discussed in Section 3.3). This ellipse does not cover the concentration of diffuse gas northeast of NGC 4410D, which may be background emission. The extracted spectrum is displayed in Figure 12a (solid line), along with the background counts from the Markevitch deep fields, reprojected and scaled to our observations (dotted line). This comparison shows that essentially all of the observed counts below 2 keV are due to the background, as are the two apparent ‘spectral features’ seen in the raw data at 1.8 and 2 keV (see also Figure 4 in Strickland et al. (2002)). This background spectrum is consistent with, but higher signal/noise than, spectra for selected regions at the edge of our field where little diffuse emission is seen.

The background-subtracted spectrum for the diffuse intragroup gas is shown in Figure 12b. Excluding energies above 1.8 keV and below 0.6 keV, where the background subtraction and calibration are more uncertain, fitting this spectrum with a Mekal function gives $kT = 0.69 \pm 0.15_{-0.16}^{+0.15}$ keV and a metallicity of $0.025 \pm 0.023_{-0.024}^{+0.023}$ solar. The total 0.3 – 8 keV luminosity of this diffuse gas is 10^{41} erg s $^{-1}$.

3.3. Point Sources

Depending upon the exact spectral shape, our observations are sensitive to point sources at the distance of NGC 4410 with 0.5 – 8 keV luminosities of $\geq 10^{39}$ erg s $^{-1}$. To search for

such sources, we used the CIAO *wavedetect* routine. In addition to the galactic nuclei and the bright bridge source, we detected 8 candidate sources in the vicinity of NGC 4410 (see Figure 13, where they are marked on the optical DSS image). These sources are listed in Table 2, along with counts in six different energy bands. None of these sources show evidence of variability, although the brightest only has 31 counts.

The first three energy bands listed in Table 2, E_1 (0.5 – 0.95 keV), E_2 (0.95 – 1.5 keV), and E_3 (1.5 – 8 keV), are expected to have equal counts for a $\Gamma = 2$ power law and nominal absorption ($N_H \sim 5 \times 10^{20} \text{ cm}^{-2}$). This table shows that source p8 has a hard spectrum, with no photons below 4 keV. Source p3 also has an over-abundance of hard photons relative to a $\Gamma = 2$ power law and nominal absorption. It is roughly consistent with a $\Gamma = 1$ power law.

Source p5 is coincident with a small angular size galaxy in the DSS image (see Figure 13), named ANON 3 in Smith (2000). No redshift is available for this object, so it is unclear at present whether it is a background galaxy or a dwarf galaxy in the NGC 4410 group. Of the remaining sources, source p2 appears to be associated with an optical concentration in the southeastern stellar tail (see Figure 13), p4 lies in the A/B–C bridge near the bright bridge source b1, p6 is north of the star forming ring, and p7 may be associated with the northwestern tail of NGC 4410A. Source p1 is closest to the galactic nuclei, at a projected distance of 27 kpc from the nucleus of NGC 4410A. Sources p1, p4, and p6, which are in the field of view of the $H\alpha$ map of Donahue et al. (2002), are not associated with H II regions. The southeastern and northwestern tails, including sources p2, p3, p7, and p8, were not in the field of view of the Donahue et al. (2002) $H\alpha$ image.

In Figure 7, the 4.9 GHz radio contours of Hummel et al. (1986) are superposed on the Chandra 0.3 – 8 keV map. Notice that the radio contours distinctly bend around source p1, so we speculate that this object may be a radio source as well. This possibility should be tested with higher resolution radio data. In addition, a radio point source at the location of p3 was found by Hummel et al. (1986) (named ‘Knot G’ by Hummel et al. (1986)). Although the contours in Figure 7 are not exactly coincident, the coordinates obtained from high resolution observations for Knot G by Hummel et al. (1986) do exactly coincide with p3. At the time of the Hummel et al. (1986) radio observations, Knot G had a flat/inverted radio spectrum with $\alpha = -0.5 \pm 0.3$, consistent with some hard state galactic black hole candidates (Corbel et al. 2000). As noted above, this source has a hard spectrum in the Chandra data.

We did not detect an X-ray counterpart to the type I supernova SN 1965A, which has a quoted position of $17''$ east, $10''$ north of the NGC 4410B nucleus (Kowal & Sargent 1971; Barbon, Capellaro, & Turatto 1991). Our upper limit of $\sim 10^{39} \text{ erg s}^{-1}$ for SN 1965A is

consistent with the upper limit to the X-ray luminosity of the type Ia SN 1992A of 5×10^{38} erg s $^{-1}$ (Schlegel & Petre 1993), and the measured X-ray luminosity of the type Ic supernova SN 2002ap, $\sim 10^{38}$ erg s $^{-1}$ (Sutaria et al. 2003). Historical type II supernova typically have X-ray luminosities of $\sim 10^{38} - 5 \times 10^{39}$ erg s $^{-1}$ (i.e., Kaaret (2001), Schlegel et al. (1996)).

4. Discussion

4.1. The Galaxies

The 0.3 – 8 keV luminosities for NGC 4410B, C, and D are 5×10^{39} erg s $^{-1}$, 8×10^{39} erg s $^{-1}$, and 10^{40} erg s $^{-1}$, respectively (Table 1). From the POSS generation I plates Cabanela (1999) found blue O magnitudes of 16.3 and 16.5 for NGC 4410C and D, respectively, while de Vaucouleurs et al. (1993) gives a blue magnitude of $B = 14.9$ for NGC 4410B. Using the relation between O and B magnitudes shown in Cabanela & Dickey (2002) and $M_B(\odot) = 5.48$ gives $L_B = 1.6 \times 10^{10} L_\odot$, $9.8 \times 10^9 L_\odot$, and $8.7 \times 10^9 L_\odot$ for NGC 4410B, C, and D. These luminosities are consistent with the Fabbiano, Kim, & Trinchieri (1992) L_X/L_B relationship for normal spiral galaxies.

The galaxy ANON 3, which has a flattened appearance on the DSS images, has an O magnitude of 19.3 (Cabanela 1999). Thus, if it is at the distance of NGC 4410, it has a blue magnitude of only $4.9 \times 10^8 L_\odot$. This implies an X-ray excess of a factor of 14 above the Fabbiano, Kim, & Trinchieri (1992) relation for normal spirals. This is unexpectedly large for such a low blue luminosity galaxy, suggesting that instead it may be a background galaxy, perhaps with an active nucleus.

4.2. The Intragroup Emission and the Group Evolutionary State

The luminosity of the intragroup medium, 10^{41} erg s $^{-1}$, is at the lower end of the range for the elliptical-dominated groups studied by Mulchaey & Zabludoff (1998), which typically have $L_x \sim 10^{41} - 5 \times 10^{42}$ erg s $^{-1}$. This supports the idea that the NGC 4410 group is in the process of evolving from a spiral-dominated group (which typically have no X-ray-emitting intragroup medium) to an elliptical-dominated group. The Chandra X-ray surface brightness gives an average density of this intragroup gas of 2×10^{-4} cm $^{-3}$, assuming standard cooling functions (McKee & Cowie 1977; McCray 1987), a temperature of 0.75 keV, and a spherical distribution with a radius of 78 kpc. The total mass of this component is $\sim 1.1 \times 10^{10} M_\odot$.

The galaxies in the inner portion of the NGC 4410 group appear to be somewhat deficient

in HI compared to their blue luminosities and morphological types (Smith 2000). This HI deficiency is likely due to gravitational interactions between the galaxies, rather than ram pressure stripping by an intracluster medium. The morphology of the HI in the group is consistent with tidal stripping (Smith 2000). Assuming the galaxies are moving at the luminosity-weighted velocity dispersion in the group of 225 km s^{-1} (Smith 2000), an estimate of the intragroup medium density required to ram pressure strip the HI based on the Gunn & Gott (1972) criteria is about 100 times larger than the density inferred from the Chandra observations.

Verdes-Montenegro et al. (2001) conducted a large HI survey of compact groups, and found significant HI deficiency compared to the field. As we found for NGC 4410, for their groups Verdes-Montenegro et al. (2001) concluded the HI deficiency was likely due to interactions rather than stripping by ram pressure. They suggest an evolutionary scenario for groups, in which interactions create HI-rich tidal features, while depleting the inner galaxies of HI. The HI in the tails is then ionized, causing the group as a whole to become deficient in HI. The HI in the NGC 4410 group is mostly found in tidal features (Smith 2000), putting NGC 4410 in a later stage in this evolutionary sequence.

The galaxies in the inner part of the NGC 4410 group are likely in the process of merging to form a central dominant elliptical. The peculiar Sab galaxy NGC 4410A is by far the most luminous galaxy in the group at optical wavelengths, contributing $\sim 25\%$ of the blue luminosity, and having an absolute blue magnitude of -21.1 , approaching that of M87 (Smith 2000). At present, NGC 4410A contains $4 \times 10^9 M_{\odot}$ of molecular gas and $\sim 10^9 M_{\odot}$ of atomic hydrogen (Smith 2000). As the system evolves, it is likely that much of this neutral gas will be used up in star formation or ionized by star formation, shocks, or the active nucleus. If this gas is converted into X-ray-emitting intragroup gas, it will boost the X-ray luminosity to $\sim 1.5 \times 10^{41} \text{ erg s}^{-1}$. After the final merger, this system may resemble the isolated elliptical NGC 1132, which is surrounded by an X-ray halo (Mulchaey & Zabludoff 1999). Since clusters of galaxies appear to form hierarchically, from the accretion of small groups (Binggeli 1993; Zabludoff & Zaritsky 1995), it is likely that the central dominant galaxies now seen in galaxy clusters originally formed in groups by a process similar to that now occurring in NGC 4410.

In some of its properties the NGC 4410 group resembles the groups HCG 16 and HCG 92 (Stephan’s Quintet). All three of these groups contain strongly interacting galaxies, with tidal tails and bridges, most of which are classified as spirals or S0s in NED. Like the NGC 4410 group, both HCG 16 and NCG 92 have X-ray-emitting intragroup gas, with similar X-ray luminosities, temperatures, and inferred abundances (Belsole et al. 2003; Trinchieri et al. 2003). There are some differences between these groups, however. HCG 16 has a higher

HI mass than the inner part of the NGC 4410 group, with $M_{HI} \sim 4 \times 10^{10} M_{\odot}$, and HI is present in both tidal features and in the inner parts of the galaxies (Verdes-Montenegro et al. 2001). This suggests that HCG 16 is in an earlier evolutionary stage than the NGC 4410 group. Stephan’s Quintet has more HI than the NGC 4410 inner group, with about $10^{10} M_{\odot}$ (Verdes-Montenegro et al. 2001), although, like NGC 4410 but unlike HCG 16, the HI in Stephan’s Quintet is mostly in the tidal features. Thus Stephan’s Quintet may be in an evolutionary stage between that of HCG 16 and the NGC 4410 group.

There are also differences in X-ray morphology. In Stephan’s Quintet, much of the diffuse X-ray-emitting gas lies in a narrow north-south ridge running through the group (Trinchieri et al. 2003). Trinchieri et al. (2003) suggests that this feature is a shock front caused by a high velocity intruder galaxy entering the group. The diffuse gas in the NGC 4410A group is somewhat elongated, but not to the extent seen in Stephan’s Quintet, while the gas in HCG 16 has a more relaxed appearance (Belsole et al. 2003).

Of these three groups, only NGC 4410 contains a radio galaxy with radio lobes that extend beyond the optical galaxy. However, the optically-brightest galaxies in HCG 16 and Stephan’s Quintet are both Seyfert galaxies (Ribeiro et al. 1996; Huchra et al. 1982). NGC 7319, the brightest galaxy in Stephan’s Quintet, has a small (2 kpc diameter) triple radio structure similar to those of FR II radio galaxies, with a flat-spectrum core and two asymmetric extended lobes (Xanthopoulos et al. 2002). This structure may be due to the interaction of radio jets with the interstellar medium in NGC 7319 (Xanthopoulos et al. 2002). Thus NGC 7319 may eventually evolve into a classical double-lobed radio galaxy.

The NGC 4410A radio lobes may have played a role in the evolution of the group as a whole. They may have been disturbed by the interstellar medium during the gravitational interaction, and may in turn have affected the gas around them. As discussed in Smith (2000), the density of intragroup medium in the NGC 4410 group is likely too small to account for the distortion of the radio lobes, implying that the distortion is probably due to the interstellar material. Radio jets may also contribute to heating the interstellar/intracluster medium (Begelman 2001; Reynolds, Heinz, & Begelman 2002).

The existence of large radio lobes in the merging galaxy NGC 4410A shows that such structures can occur fairly early in the formation of an elliptical, when it is not yet an elliptical. NGC 4410A thus stands in contrast to the three ‘compact symmetric object’ radio galaxies studied by Perlman et al. (2001), which have normal outer optical isophotes but significant ellipticity and position angle variations in the inner region. In these three galaxies, the optical morphology suggests that a major merger occurred $\geq 10^8$ years ago, while the radio morphology indicates a recent ($10^3 - 10^4$ years) turn-on of jet activity, implying a time delay between such a merger and jet activity. This may mean that minor mergers,

which will not drastically alter the outer isophotes, may also trigger jet activity, or that jet activity is intermittent in elliptical galaxies, as suggested by Reynolds & Begelman (1997) and McNamara et al. (2001), or that jets can also be present in spirals but are generally smothered by dense interstellar clouds (Wang, Wiita, & Hooda 2000), as suggested for NGC 7319 (Xanthopoulos et al. 2002). Once formed, jets may affect the evolution of the interstellar and intragroup gas, providing periodic heating to the interstellar and intracluster/intragroup gas.

4.3. The NGC 4410A Ring and the Diffuse X-Ray Emission in NGC 4410A

The peculiar ring-like structure visible in optical images of NGC 4410A (Figure 2, Donahue et al. (2002)) is reminiscent of those in classical ring galaxies (Lynds & Toomre 1976; Theys & Spiegel 1977). The existence of luminous H II regions along the ring is also consistent with a collisional ring scenario, as such H II regions are often found in classical ring galaxies (e.g., Higdon (1995)). However, the optical spectrum of the western edge of the NGC 4410 ring is indicative of shocks (Donahue et al. 2002), which is not typical of ring galaxies (Jeske 1986; Bransford et al. 1998).

The detection of extended x-ray emission along the western half of the NGC 4410 ring provides another test of the collisional-ring hypothesis. NGC 4410 is not the only ring(-like) galaxy with X-rays detected along the optical ring. ROSAT images of the Cartwheel (Wolter, Trinchieri, & Iovino 1999) show X-rays along the southwestern portion of the ring, with an X-ray luminosity of $2 - 3 \times 10^{41} \text{ erg s}^{-1}$. Higher resolution Chandra observations of the Cartwheel show that this X-ray emission is largely due to point sources, with about $10^{40} \text{ erg s}^{-1}$ being due to diffuse gas (Wolter & Trinchieri 2003). This is similar to our measurement of $L_X = 6 \times 10^{39} \text{ erg s}^{-1}$ for the ridge of X-ray emission along the western part of the NGC 4410 ring. However, in contrast to NGC 4410, in the Cartwheel the part of the ring brightest in x-rays also has the most star formation (Higdon 1995; Wolter, Trinchieri, & Iovino 1999), while in NGC 4410, the western part of the ring is detected in X-rays, and the H II regions are located in the eastern part (Figure 2, Donahue et al. (2002)).

The extended X-ray emission in both the Cartwheel and NGC 4410 is unlikely to be due to shocks from an expanding density wave caused by a collision with another galaxy. Typical expansion velocities for collisional rings are $50 - 100 \text{ km s}^{-1}$ (Struck-Marcell & Higdon 1993; Gerber, Lamb, & Balsara 1996). As discussed by Wolter, Trinchieri, & Iovino (1999), such velocities imply very low gas temperatures of $\sim 50 \text{ eV}$. Such low temperatures would cause strong line emission in the extreme ultraviolet, rather than a dominant X-ray continuum (McCray 1987).

Although shocks from an expanding density wave are not likely to have caused the diffuse X-rays directly, they may be indirectly responsible, arising as a consequence of star formation triggered by an expanding ring. Alternatively, star formation triggered by another process may be responsible for the diffuse X-rays in this system. The total X-ray luminosity in the diffuse component in NGC 4410A+B, compared to other star formation indicators, is consistent with that expected from star formation. The far-infrared luminosity of NGC 4410A+B is $3.9 \times 10^9 L_{\odot}$ (Smith 2000). Comparison with the total diffuse X-ray emission in NGC 4410A+B of $6 \times 10^{40} \text{ erg s}^{-1}$ gives a ratio consistent with the David, Jones, & Forman (1992) and Stevens & Strickland (1998) L_X vs. L_{FIR} relationships for star forming galaxies, thus NGC 4410 does not have a large excess of diffuse X-ray emitting gas compared to normal star forming galaxies. Another useful comparison is with the non-nuclear $H\alpha$ luminosity of NGC 4410A+B, $1.7 \times 10^{41} \text{ erg s}^{-1}$ (Donahue et al. 2002). The diffuse $L_X/L_{H\alpha} \sim 0.35$ is consistent with global values for starburst galaxies (Pérez-Olea & Colina 1996). The total diffuse X-ray luminosity in NGC 4410A is similar to the soft X-ray luminosity found in the prototypical spiral-to-elliptical merger NGC 7252 (Awaki, Matsumoto, & Tomida 2002).

The extended x-ray emission in NGC 4410A (and in other star-forming galaxies) is not likely to be due to supernova remnants alone. The typical X-ray luminosity of a supernova remnant is $10^{36} \text{ erg s}^{-1}$, while its lifetime is about 2×10^4 years (Cowie et al. 1981). Comparison with the observed X-ray luminosity of the NGC 4410 ring implies a supernova rate of 0.3 per year, if all the X-ray emission in the ridge is due to supernovae. If the total diffuse X-ray emission in NGC 4410A+B, $L_X \sim 6 \times 10^{40} \text{ erg s}^{-1}$, is assumed to be due to supernovae, the implied supernova rate is even higher, at 3 supernovae per year. These implied rates are high compared to the total rate of star formation in NGC 4410A, $1 - 4 M_{\odot} \text{ year}^{-1}$ (Donahue et al. 2002) (which in any case is mainly observed in the eastern portion of NGC 4410A, not along the western arc). Expected supernova rates, relative to star formation rates, are $\sim 0.03 \text{ supernova}/(M_{\odot} \text{ year}^{-1})$ (Taniguchi et al. 2001), thus, based on the non-nuclear $H\alpha$ luminosity, we expect only $0.03 - 0.12$ supernova per year in NGC 4410A. In general, supernova remnants are believed to contribute only a small amount to the X-ray emission from starburst galaxies (Peris & Rephaeli 2002).

A related phenomenon more likely to be responsible for the diffuse X-ray emission is the combined effect of stellar winds from massive stars and supernovae, creating an expanding bubble of hot gas. Expansion of the bubble may shock the surrounding gas, contributing to the X-ray radiation. Such superbubbles in starburst galaxies may be capable of generating up to $L_X \sim 10^{39-41} \text{ erg s}^{-1}$ (Stevens & Strickland 1998). Chandra observations of the starburst galaxy NGC 253 (Strickland et al. 2000) reveal a $\sim 0.5 \text{ kpc}$ radius conical-shaped outflow from the nucleus, with an edge-brightened X-ray morphology similar to that seen in $H\alpha$. Strickland et al. (2000) conclude that the diffuse X-rays from NGC 253 originate

from an interface region between the wind and the ambient interstellar medium. In the SBc galaxy NGC 3079, a 0.6 kpc radius superbubble is seen, with matching X-ray and optical line morphologies (Cecil, Bland-Hawthorn, & Veilleux 2002). The X-ray luminosity associated with this bubble is 3×10^{42} erg s⁻¹, 50 times higher than the total extended X-ray luminosity of NGC 4410A+B. In NGC 3079, unlike in NGC 253, the X-rays are not significantly edge-brightened, and the cause of the superbubble (AGN or starburst) is not clear.

The western arc/X-ray ridge in NGC 4410, however, is much larger than the superbubbles in these galaxies, extending ~ 4 kpc from the nucleus. The expansion timescale of a superbubble can be estimated from $t_7^{-3/5} \sim 2.8 L_{mech}^{1/5} n_H^{-1/5} / r_{shell}$, where t_7 is the timescale in units of 10^7 years, L_{mech} is the mechanical energy of the supernova in units of 10^{43} erg s⁻¹, n_H is the average hydrogen number density in units of 1 cm^{-3} , and r_{shell} is the radius of the bubble in kpc (Shull 1995; Taniguchi et al. 2001). Using $L_{mech} \sim \eta E_{SN} R_{SN}$, where $\eta \sim 0.1$ is the efficiency of the kinetic energy deposited into the gas (Dyson & Williams 1980), $E_{SN} \sim 10^{51}$ erg is the energy of a single supernova, R_{SN} is the number of supernova per year, and the hydrogen number density $n_H \sim 1 \text{ cm}^{-3}$ gives $L_{mech} \sim 0.9 - 3.9 \times 10^{41}$ erg s⁻¹, using the supernova rate implied by the H α luminosity. This implies a timescale of $5 - 9 \times 10^7$ years for the bubble.

If the X-ray/optical emission-line arc in NGC 4410 was indeed caused by a superbubble, it might be caused by the active nucleus rather than by star formation. Theoretical models of a radio jet impacting the interstellar medium or intragroup medium predict an X-ray shell surrounding the radio lobes (Reynolds, Heinz, & Begelman 2001). Such shells are observed in a number of radio galaxies (Carilli, Perley, & Harris 1994; Böhringer et al. 1993; Huang & Sarazin 1998). Unfortunately, at present no high spatial resolution, high sensitivity radio observations are available for NGC 4410A for comparison with the Chandra data. In the 1986 maps of Hummel et al. (1986), only the southern radio lobe is visible. In the higher sensitivity but low spatial resolution map of Smith (2000), a second lobe is visible, but its detailed morphology is uncertain. Thus at present it is unclear whether or not the X-ray ridge in NGC 4410A bounds a radio lobe.

4.4. The Point Sources

As discussed above, of the eight point sources found in the NGC 4410 field, one of them (p5) is associated with the faint optical galaxy ANON 3, and may be a background source. The second source with an optical counterpart, p2, may also be a background source. The optical counterpart is too faint to have been included in the Cabanella (1999) catalog of

POSS I sources, however, it is clearly visible on the POSS II plates. Roughly calibrating these images by comparison with the Cabanela (1999) galaxy magnitudes, we estimate $B \sim 19.5$ and $V \sim 19$ for the optical counterpart to p2. At the distance of NGC 4410, this corresponds to a blue luminosity of $2.4 \times 10^8 L_\odot$ ($M_B \sim -15.4$ and $M_V \sim -15.9$). This is much more luminous in the visible than almost all of the so-called ‘super star clusters’ found in star-forming galaxies (*e.g.*, Holtzman et al. (1992, 1996)). This source has a $\log(F_X/F_V)$ ratio of -1.4 (calculated as in Maccacaro et al. (1988)), much smaller than that of the apparent optical counterparts to some Ultraluminous X-ray sources (ULXs) found in other galaxies. For example, the apparent optical counterparts to ULXs found in M82 and NGC 4565 have $M_B \sim -5$ and $\log(F_X/F_V) \sim 2$ (Stocke, Wurtz, & Kühr 1991; Wu et al. 2002).

Thus p2 is clearly not in the same class as these ULXs, being much brighter in the optical (if the POSS optical source is indeed related to the X-ray source). It is more likely to be a background active galaxy. Although luminous in the optical compared to these other ULXs, it is faint in the optical relative to the X-ray compared to normal galaxies; it lies above the Fabbiano, Kim, & Trinchieri (1992) L_X/L_B relation for normal galaxies. If it is at the distance of NGC 4410, its optical luminosity is typical of a dwarf galaxy. As argued earlier for ANON 3, it is unlikely that such a low luminosity galaxy would harbor an active galaxy. Thus p2 may also be a background object.

The remaining six candidate ULXs without optical counterparts on the POSS images have lower limits to $\log(F_X/F_V)$ between -1.5 to -0.4 , assuming an optical limit of $V \sim 20.5$ from the POSS I plates. These limits are not sensitive enough to distinguish between ULXs and background active galaxies, via comparison with typical values for BL Lacs and other AGNs (*i.e.*, Stocke et al. (1991)).

As discussed in Section 3.3, two of our candidate ULXs, p3 and p8, have hard X-ray spectra compared to a $\Gamma = 2$ power law. Candidate ULXs in other galaxies typically have spectra consistent with $\Gamma \sim 2$ power laws (Roberts et al. 2001; Lira et al. 2002), though there is some evidence for harder spectra ($\Gamma \sim 1.2$) among the more luminous ULXs (Zezas et al. 2002). Thus p3 and p8 may also be background sources (Seyfert 2, for example). Alternatively, they may be ‘microquasars’, particularly p3, whose large radio flux may indicate that we are viewing nearly straight down the jet axis of a ‘microquasar’ such as GRS 1915+105. Intriguingly, p3 and p8 are spatially located together southeast of NGC 4410A near p2, which has an optical counterpart. If these are indeed all background objects, they may be part of a background cluster. Alternatively, they may be ULXs associated with the NGC 4410 tidal tail.

Thus, our four best candidate ULX sources are p1, p4, p6, and p7. Given the star formation rate estimate for NGC 4410A of $1 - 4 M_\odot \text{ year}^{-1}$ (Donahue et al. 2002), we expect to

find 1 – 4 ULXs associated with NGC 4410A, if ULXs follow a universal luminosity function dependent upon star formation rate, as suggested by Grimm, Gilfanov, & Sunyaev (2003). Our detection of four possible candidates in NGC 4410 is consistent with this expectation. As noted above, however, three of these sources (p1, p4, and p6) are not associated with known star formation regions.

The possible association of radio emission with one of these candidate ULXs, p1, is intriguing. To date, only one other ULX with a possible radio counterpart has been found (Kaaret et al. 2003). If these objects are indeed radio-bright ULXs, this suggests that they are not intermediate mass black holes, but instead beamed stellar mass objects (Kaaret et al. 2003). Alternatively, p1 may be a background radio-loud active galaxy.

5. Summary

The peculiar galaxy NGC 4410A contains a X-ray-bright active nucleus as well as diffuse extended emission, including a ridge of X-ray emission coincident with optical line emission. This ridge has an optical spectrum indicative of shocks, suggesting it may be the rim of an expanding superbubble caused by either the on-going star formation in NGC 4410A or its active nucleus. Outside of the optical galaxies in the group, a hot intragroup gas with $L_X \sim 10^{41}$ erg s $^{-1}$ is observed, at the lower edge of the range observed for elliptical-dominated groups. This suggests that the NGC 4410 group is in the process of evolving from a spiral-dominated group into an elliptical-dominated group. Four or five possible ULXs are seen in the Chandra maps of NGC 4410A, one of which has a possible radio counterpart. Such a radio counterpart argues against the intermediate mass black hole model for this source, and supports the hypothesis that this is simply a beamed stellar-mass binary.

We thank the Chandra team for making this research possible. This research has made use of the NASA/IPAC Extragalactic Database (NED) which is operated by the Jet Propulsion Laboratory, California Institute of Technology, under contract with the National Aeronautics and Space Administration. We appreciate the helpful suggestions of the anonymous referee. We thank Anna Wolter for helpful comments on the manuscript, and for providing information on the Cartwheel Chandra observations in advance of publication. We also thank Kathy Manning and John Houck for advice with the data reduction software. We are pleased to acknowledge funding for this project from a NASA General Observer Chandra grant. M.A.N. was supported by NASA grant NAS8-01129.

REFERENCES

- Awaki, H., Matsumoto, & Tomida, H. 2002, ApJ, 567, 892
- Barbon, R., Capellaro, E., & Turatto, M. 1991, in *Supernovae: The Tenth Santa Cruz Workshop in Astronomy and Astrophysics*, ed. S. E. Woosley (Springer-Verlag, New York), p. 720.
- Barnes, J.E. 1985, MNRAS, 215, 517
- Barnes, J.E. & Hernquist, L. 1992, ARAA, 30, 705
- Begelman, M. C. 2001, in Proceedings of the Gas and Galaxy Evolution Conference, ASP Conference Series, vol. 240, p. 363
- Belsole, E., Sauvageot, J.-L., Ponman, T. J., & Bourdin, H. 2003, A&A, 398, 1
- Binggeli, B. 1993, A&A, 98, 275
- Böhringer, H., Voges, W., Fabian, A. C., Edge, A. C., & Neumann, D. M. 1993, MNRAS, 264, L25
- Borne, K. D. & Colina, L. 1993, ApJ, 416, 157
- Bransford, M. A., Appleton, P. N., Marston, A. P., & Charmandaris, V. 1998, AJ, 116, 2757
- Cabanela, J. E. 1999, Ph.D. Thesis, University of Minnesota.
- Cabanela, J. E., & Dickey, J. M. 2002, AJ, 124, 78
- Carilli, C. L., Perley, R. A., & Harris, D. E. 1994, MNRAS, 270, 173
- Cecil, G., Bland-Hawthorn, J., & Veilleux, S. 2002, ApJ, 576, 745
- Corbel, S., Fender, R. P., Tzioumis, A. K., Nowak, M., McIntyre, V., Durouchoux, P., & Sood, R. 2000, A&A, 359, 251
- Cowie, L. L., McKee, C. F., & Ostriker, J. P. 1991, ApJ, 247, 908
- David, L. P., Jones, C., & Forman, W. 1992, ApJ, 388, 82
- De Young, D. S. 1981, Nature, 293, 43
- de Vaucouleurs, G., de Vaucouleurs, A., Corwin, H. G., Jr., Buta, R. J., Paturel, G., & Fouque, P. 1993, Third Reference Catalogue of Bright Galaxies (Berlin: Springer)

- Dickey, J. M. & Lockman, F. J. 1990, ARAA, 28, 215
- Donahue, M., Smith, B. J., & Stocke, J. T. 2002, AJ, 123, 1922
- Dyson, J. E., & Williams, D. A. 1980, Physics of the Interstellar Medium (Manchester: Manchester Univ. Press).
- Fabbiano, G., Kim, D. W., & Trinchieri, G., 1992, ApJS, 80, 531
- Gerber, R. A., Lamb, S. A., & Balsara, D. S. 1996, MNRAS, 278, 345
- Grimm, H.-J., Gilfanov, M., & Sunyaev, R. 2002, MNRAS, 339, 793
- Gunn, J. E., & Gott, J. R. III 1972, ApJ, 176, 1.
- Higdon, J. L. 1995, ApJ, 455, 524
- Holtzman, J. A., et al. 1992, AJ, 103, 691
- Holtzman, J. A., et al. 1996, AJ, 112, 416
- Houck, J. C. & Denicola, L. A. 2000, ASP Conf. Ser. 216: Astronomical Data Analysis Software and Systems IX, 9, 591.
- Huchra, J. P., Wyatt, W. F., & Davis, M. 1982, AJ, 87, 1628
- Hummel, E., Kotanyi, C. G., and van Gorkom, J. H. 1986, AA, 155, 161
- Huang, Z., & Sarazin, C. L. 1998, ApJ, 496, 728
- Jeske, N. A. 1986, Ph.D. thesis, University of California, Berkeley
- Kaaret, P. 2001, ApJ, 560, 715
- Kaaret, P., Corbel, S., Prestwich, A. H., & Zezas, A. 2003, Science, 299, 365
- Kowal, C. T., & Sargent, W. L. W. 1971, AJ, 76, 756
- Lira, P., Ward, M., Zezas, A., Alonso-Herrero, A., & Ueno, S. 2002, MNRAS, 330, 259
- Lynds, R., & Toomre, A. 1976, ApJ, 209, 382
- Maccacaro, T., Gioia, I., Wolter, A., Zamorani, G., & Stocke, J. 1998, ApJ, 326, 680
- Mackie, G., & Fabbiano, G. 1998, ApJ, 115, 514
- Mazzarella, J. M., & Boroson, T. A. 1993, ApJS, 85, 27

- McCray, R. 1987, in *Spectroscopy of Astrophysical Plasmas*, ed. A. Dalgarno and D. Layzer (Cambridge University Press: New York, NY), p. 260
- McKee, C. F., & Cowie, L. L. 1977, *ApJ*, 215, 213
- McNamara, B. R., et al. 2001, *ApJ*, 562, L149
- Miley, G. K., et al. 1972, *Nature*, 237, 269
- Moderski, R. & Sikora, M. 1996, *A&AS*, 120, 591
- Mulchaey, J.S. & Zabludoff, A.I. 1998, *ApJ*, 496, 73
- Mulchaey, J.S. & Zabludoff, A.I. 1999, *ApJ*, 514, 133
- Owen, F. N., & White, R. A. 1991, *MNRAS*, 249, 164
- Pérez-Olea, D. E., & Colina, L. 1996, *ApJ*, 468, 191
- Peris, M., & Rephaeli, Y. 2002, *A&A*, 382, 843
- Perlman, E. S., Stocke, J. T., Conway, J., & Reynolds, C. 2001, *ApJ*, 122, 536
- Reynolds, C. S., & Begelman, M. C. 1997, *ApJ*, 487, L135
- Reynolds, C. S., Heinz, S., & Begelman, M. C. 2001, *ApJ*, 549, L179
- Reynolds, C. S., Heinz, S., & Begelman, M. C. 2002, *MNRAS*, 332, 271
- Ribeiro, A. L. B., de Carvalho, R. R., Coziol, R., Capelato, H. V., & Zepf, S. E. 1996, *ApJ*, 463, L5
- Roberts, T. P., Goad, M. R., Ward, M. J., Warwick, R. S., O’Brien, P. T., Lira, P., & Hands, A. D. P. 2001, *MNRAS*, 325, L7
- Schlegel, E. M., & Petre, R. 1993, *ApJ*, 412, L29
- Schlegel, E. M., Petre, R., & Colbert, E. J. M. 1996, *ApJ*, 456, 187
- Shull, J. M. 1995, in *ASP Conf. Ser. 73, Airborne Astronomy Symp. on the Galactic Ecosystem*, ed. M.R. Haas, J. A. Davidson, & E. F. Erickson (San Francisco: ASP), 365
- Smith, B. J. 2000, *ApJ*, 541, 624
- Stocke, J. T., and Burns, J. O. 1987, *ApJ*, 319, 671

- Stocke, J. T., Burns, J. O., and Christiansen, W. A. 1985, *ApJ*, 299, 799
- Stocke, J. T., Wurtz, R., & Kühr, H. 1991, *AJ*, 102, 1724
- Stevens, I. R., & Strickland, D. K. 1998, *MNRAS*, 294, 523
- Stocke, J. T., Morris, S. L., Giola, I. M., Maccacaro, T., Schild, R., Wolter, A., Fleming, T. A., & Henry, J. P. 1991, *ApJS*, 76, 813
- Strickland, D. K., Heckman, T. M., Weaver, K. A., & Dahlem, M. 2000, *ApJ*, 120, 2965
- Strickland, D. K., Heckman, T. M., Weaver, K. A., Hoopes, M., & Dahlem, M. 2002, *ApJ*, 568, 689
- Struck-Marcell, C., & Higdon, J. L. 1993, *ApJ*, 411, 108
- Sutarai, F. K., Chandra, P., Bhatnagar, S., & Ray, A. 2003, *A&A*, 397, 1011
- Taniguchi, Y. et al. 2001, *ApJ*, 559, L9
- Theys, J. C., & Spiegel, E. A. 1977, *ApJ*, 212, 616
- Trinchieri, G., Sulentic, J., Breitschwerdt, D., & Pietsch, W. 2003, *A&A*, in press (astro-ph/0302590)
- Tschöke, D., Hensler, G., & Junkes, N. 1999, *A&A*, 343, 373
- Van Breugel, W. J. M., et al. 1985, *ApJ*, 293, 83
- Van Breugel, W. J. M., et al. 1986, *ApJ*, 311, 58
- Verdes-Montenegro, L., Yun, M. S., Williams, B. A., Huchtmeier, W. K., Del Olmo, A., & Perea, J. 2001, *A&A*, 377, 812
- Wang, J., Wiita, P. J., & Hooda, J. S. 2000, *ApJ*, 539, 201
- Weisskopf, M. C., Brinkman, B., Canizares, C., Carmire, G., Murray, S., & Van Speybroeck, L. P. 2002, *PASP*, 114, 1
- Wilson, A. S. & Colbert, E. J. M. 1995, *ApJ*, 438, 62
- Wolter, A., & Trinchieri, G. 2003, *Proceedings of the XLVII Congresso Nazionale SAI* 2003, ed. L. Girardi and S. Zaggia
- Wolter, A., Trinchieri, G., & Iovino, A. 1999, *A&A*, 342, 41

Wu, H., Xue, S. J., Xia, X. Y., Deng, Z. G., & Mao, S. 2002, *ApJ*, 576, 738

Xanthopoulos, E., Muxlow, T. W. B., Thomasson, P., & Garrington, S. T. 2002, *MNRAS*, submitted (astro-ph/0202332).

Zabludoff, A. I., & Zaritsky, D. 1995, *ApJ*, 447, L21

Zezas, A., Fabbiano, G., Rots, A. H., & Murray, S. S. 2002, *ApJS*, 142, 239

Fig. 1.— An optical R-band image of the inner part of the NGC 4410 galaxy group, obtained with the South Eastern Association for Research in Astronomy (SARA) 0.9 m telescope (from Smith 2000, Donahue et al. 2002). The stretch is set to emphasize the faint bridges connecting NGC 4410 A+B with NGC4410 C and NGC 4410 D, as well as the long tail extending to the southeast of NGC 4410 A+B. The field of view of this image is $\approx 6.7 \text{ arcmin} \times 6.3 \text{ arcmin}$ (slightly smaller than the ACIS-S S3 chip). North is up and east is to the left.

Fig. 2.— A closer view of NGC 4410 A+B (from Donahue et al. 2002). The left image is a red continuum image, while the right image is an $H\alpha$ + $[N\ II]$ image. The field of view is $\approx 0.8\text{ arcmin} \times 1.1\text{ arcmin}$. NGC 4410A, the galaxy on the right in these images, has a prominent bulge surrounded by a ring-like or loop-like structure. Optical spectroscopy (Donahue et al. 2002) confirms that the bright clumps in the ring and the extremely bright knot southwest of the NGC 4410A nucleus are extremely luminous H II regions, however, the arc to the northwest of the NGC 4410 nucleus has an optical spectrum indicative of shocks. The most luminous H II region is twice as luminous as 30 Doradus. The registration on these images has been adjusted to match the Chandra and Hummel et al. (1986) radio continuum positions of the nucleus of NGC 4410A.

Fig. 3.— The final Chandra 0.3 – 8 keV image (greyscale), superposed on the optical Digitized Sky Survey (DSS) image (contours). Note the X-ray counterparts to NGC 4410A+B, NGC 4410C, and NGC 4410D, as well as numerous background sources. This map was made using an exposure map that was weighted using the spectrum of a $57''.5 \times 40''$ region enclosing the NGC 4410A+B complex. Note that the morphology of the extended emission does not vary with different assumptions used in making the exposure map.

Fig. 4.— The low energy (0.3 – 1 keV) Chandra image of the inner portion of the NGC 4410 group (greyscale). This map was made using a monochromatic 0.8 keV exposure map. As in the previous figure, the contours are from the optical Digitized Sky Survey (DSS) image. Note the possible faint X-ray counterpart to NGC 4410F.

Fig. 5.— The middle energy (1 – 2.5 keV) Chandra image of the inner portion of the NGC 4410 group (greyscale). This map was made using a monochromatic 1.5 keV exposure map. As in the previous figures, the contours are from the optical Digitized Sky Survey (DSS) image.

Fig. 6.— The high energy (2.5 – 8 keV) Chandra image of the inner portion of the NGC 4410 group (greyscale). This map was made using a monochromatic 3 keV exposure map. As in the previous figures, the contours are from the optical Digitized Sky Survey (DSS) image.

Fig. 7.— The Hummel et al. (1986) 4.9 GHz radio continuum map, superposed on the 0.3 – 8 keV Chandra map.

Fig. 8.— The Chandra 0.3 – 8 keV image of the NGC 4410A+B region. The bright source is centered on the nucleus of NGC 4410A, while the secondary source to the east is associated with the nucleus of NGC 4410B. The extension to the northwest is coincident with the shock-ionized optical emission line gas seen in the $H\alpha$ map (Figure 2).

Fig. 9.— Left: A broadband red archival Hubble Space Telescope image. Right: The HST red image (contours), superposed on the unsmoothed Chandra 0.3 – 8 keV image of the NGC 4410A+B region. Note that the optically-bright knots to the southeast and northeast of the nucleus of NGC 4410A are not visible as discrete sources in the X-ray map. The extended X-ray radiation to the

northwest is concentrated along the inner edge of the optical arc.

Fig. 10.— The Chandra 0.3 – 8 keV image of the NGC 4410A+B region (greyscale), with the Donahue et al. (2002) $H\alpha$ + $[N\ II]$ image superimposed (contours). The $H\alpha$ + $[N\ II]$ image has been re-registered so that the NGC 4410A nucleus is coincident with the radio continuum and X-ray nucleus. Note the $\sim 3''$ extension to the southwest of the NGC 4410A nucleus which is present in both the X-ray and in the optical line emission. Note also that the concentration of X-ray emission $18''$ – $20''$ to the northwest of the NGC 4410A nucleus is coincident with the arc of ionized gas seen in the optical image. In addition, note that the HII regions to the southeast and northeast of the nucleus of NGC 4410A are not visible as discrete sources in the X-ray map.

Fig. 11.— a) The 0.5 – 5 keV spectrum of the inner $1''$ of NGC 4410A (solid line). The dotted line is the best fit to an absorbed power law, with the column density fixed to the nominal value. A pile-up model was assumed. b) The 0.5 – 5 keV spectrum of the $1''$ – $5''$ annulus around NGC 4410A (solid line). The dotted line is the fit to a power law plus Mekal function, as described in the text (see Table 1). c) The 0.5 – 5 keV spectrum of the $5''$ – $10''$ annulus around NGC 4410A (solid line). The dotted line is the fit to a power law plus Mekal function (see text and Table 1). d) The 0.5 – 5 keV spectrum of the bright bridge source. The dotted line is the fit to a power law function, as described in the text (see also Table 1).

Fig. 12.— a) The observed 0.5 – 5 keV spectrum of the diffuse intragroup gas in the NGC 4410 group (solid line), compared to expected background counts from the deep Markevitch observations (dotted lines). b) The background-subtracted spectrum for the diffuse gas in the NGC 4410 group (solid line), compared to the best-fit model (dotted line).

Fig. 13.— An overlay of the positions of the candidate Ultraluminous X-Ray sources (ULXs) (see Table 2), on the red Second Generation Digitized Sky Survey Image.

Table 1. Spectral Fits to X-ray Sources in the NGC 4410 Field.

Source	Function	χ^2/DoF	n_{H} $\times 10^{20} \text{ cm}^{-2}$	Γ	kT	L_X (0.3–8 keV) (10^{40} erg/s)
A ($<1''$) ^a	Power Law	15/30	5 ^b	1.96±0.10		25
A ($<1''$) ^a	Power Law	14/30	3.7± $^{1.9}_{1.7}$	1.96 ^b		23
A ($<1''$) ^a	Power Law	18/30	6.7± $^{1.9}_{1.8}$	2.1 ^b		22
A ($<1''$) ^a	Power Law	27/30	10.7± $^{1.9}_{1.8}$	2.3 ^b		20
A (1''–5'')	Mekal	2.2/9	5 ^b		0.62± $^{0.08}_{0.07}$	4.1
A (5''–10'')	Mekal	1.3/4	5 ^b		0.54± $^{0.12}_{0.14}$	1.9
B	Bremsstrahlung	–	5 ^b		0.2 ^b	0.7
C	Bremsstrahlung	–	5 ^b		0.5 ^b	0.4
D	Bremsstrahlung	–	5 ^b		0.5 ^b	0.8
b1	Power Law	1.2/6	5 ^b	2.2± $^{0.3}_{0.2}$		3.6
Intragroup Gas	Mekal	23/19	1.7 ^b		0.69 ± $^{0.15}_{0.16}$	10

^a Used pileup model with $\alpha = 0.5$ and psffract = 0.95 fixed.

^bParameter fixed.

Note. — Fits are from 0.5 – 5 keV, except in the case of the inner annulus around NGC 4410A and the diffuse intragroup gas, where 0.6 – 1.8 keV was used, and the outer NGC 4410A annulus, where the energy range was restricted to 0.6 – 1.2 keV. Before fitting, data were rebinned to 20 counts/bin. Luminosities were calculated assuming a distance of 97 Mpc. The best-fit abundances for the inner and outer annuli of NGC 4410A and the diffuse gas are $0.06 \pm ^{0.06}_{0.03}$, $0.11 \pm ^{1.16}_{0.09}$, and $0.025 \pm ^{0.025}_{0.024}$ solar, respectively.

Table 2. Counts and Luminosities of Point Sources

Source	R.A.			Dec.			E_1	E_2	E_3^a	E_A	E_B	E_C^b	L_A	L_B	L_C	Total ^c
	(J2000)			(J2000)					(Counts)					($\times 10^{39}$	erg s ⁻¹)	
P1	12	26	31.857	+9	1	1.54	7	7	17	11	14	6	$1.4^{+0.8}_{-0.6}$	$3.6^{+1.8}_{-1.4}$	$6.1^{+5.1}_{-3.3}$	$11.1^{+5.5}_{-3.6}$
P2 ^d	12	26	34.266	+8	59	35.57	6	1	8	7	6	2	$0.9^{+0.7}_{-0.5}$	$1.6^{+1.3}_{-0.8}$	$2.0^{+3.5}_{-1.6}$	$4.5^{+3.8}_{-1.8}$
P3 ^e	12	26	32.457	+8	59	32.17	1	1	7	1	6	2	$0.1^{+0.4}_{-0.1}$	$1.6^{+1.3}_{-0.8}$	$2.0^{+3.5}_{-1.6}$	$3.7^{+3.8}_{-1.8}$
P4	12	26	32.429	+9	1	41.44	1	1	3	2	3	0	$0.3^{+0.4}_{-0.2}$	$0.8^{+1.0}_{-0.5}$	$0.0^{+2.3}_{-0.0}$	$1.0^{+2.6}_{-0.6}$
P5 ^f	12	26	32.792	+9	3	0.94	2	2	3	3	4	0	$0.4^{+0.5}_{-0.3}$	$1.0^{+1.1}_{-0.6}$	$0.0^{+2.3}_{-0.0}$	$1.4^{+2.6}_{-0.7}$
P6	12	26	29.354	+9	1	54.36	2	3	4	4	4	1	$0.5^{+0.6}_{-0.3}$	$1.0^{+1.1}_{-0.6}$	$1.0^{+2.9}_{-0.9}$	$2.6^{+3.2}_{-1.2}$
P7	12	26	22.985	+9	2	4.49	1	0	4	1	3	1	$0.1^{+0.4}_{-0.1}$	$0.8^{+1.0}_{-0.5}$	$1.0^{+2.9}_{-0.9}$	$1.9^{+3.1}_{-1.1}$
P8	12	26	33.458	+8	59	39.79	0	0	4	0	0	4	$0.0^{+0.3}_{-0.0}$	$0.0^{+0.6}_{-0.0}$	$4.1^{+4.4}_{-2.5}$	$4.1^{+4.5}_{-2.5}$

^a $E_1 = 0.5\text{--}0.95$ keV, $E_2 = 0.95\text{--}1.5$ keV, $E_3 = 1.5\text{--}8$ keV. A $\Gamma = 2$ power law source absorbed by a column of $N_H = 5 \times 10^{20}$ cm⁻² should have equal counts per energy bin.

^b $E_A = 0.5\text{--}1.4$ keV, $E_B = 1.4\text{--}3.4$ keV, $E_C = 3.4\text{--}8$ keV. A $\Gamma = 2$ power law source absorbed by a column of $N_H = 5 \times 10^{20}$ cm⁻² should have equal flux per energy bin.

^cAbsorbed luminosities, determined for each bin individually, assuming a $\Gamma = 2$ power law source absorbed by a column of $N_H = 5 \times 10^{20}$ cm⁻² at a distance of 97 Mpc.

^dPossible optical counterpart on DSS.

^eCoincident with radio Knot G in Hummel et al. (1986) radio continuum map.

^fCoincident with small angular size galaxy ANON 3 on DSS image (as named in Smith 2000).

This figure "bsmith_fig1.gif" is available in "gif" format from:

<http://arxiv.org/ps/astro-ph/0307159v1>

This figure "bsmith_fig2a.gif" is available in "gif" format from:

<http://arxiv.org/ps/astro-ph/0307159v1>

This figure "bsmith_fig2b.gif" is available in "gif" format from:

<http://arxiv.org/ps/astro-ph/0307159v1>

This figure "bsmith_fig3.gif" is available in "gif" format from:

<http://arxiv.org/ps/astro-ph/0307159v1>

This figure "bsmith_fig4.gif" is available in "gif" format from:

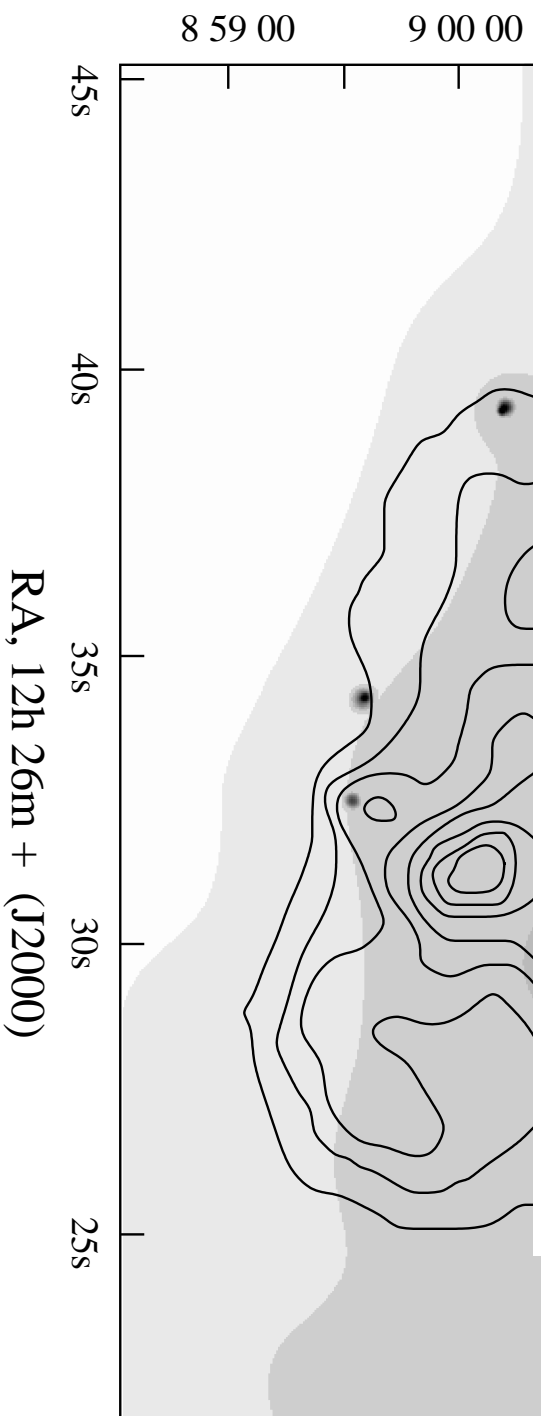
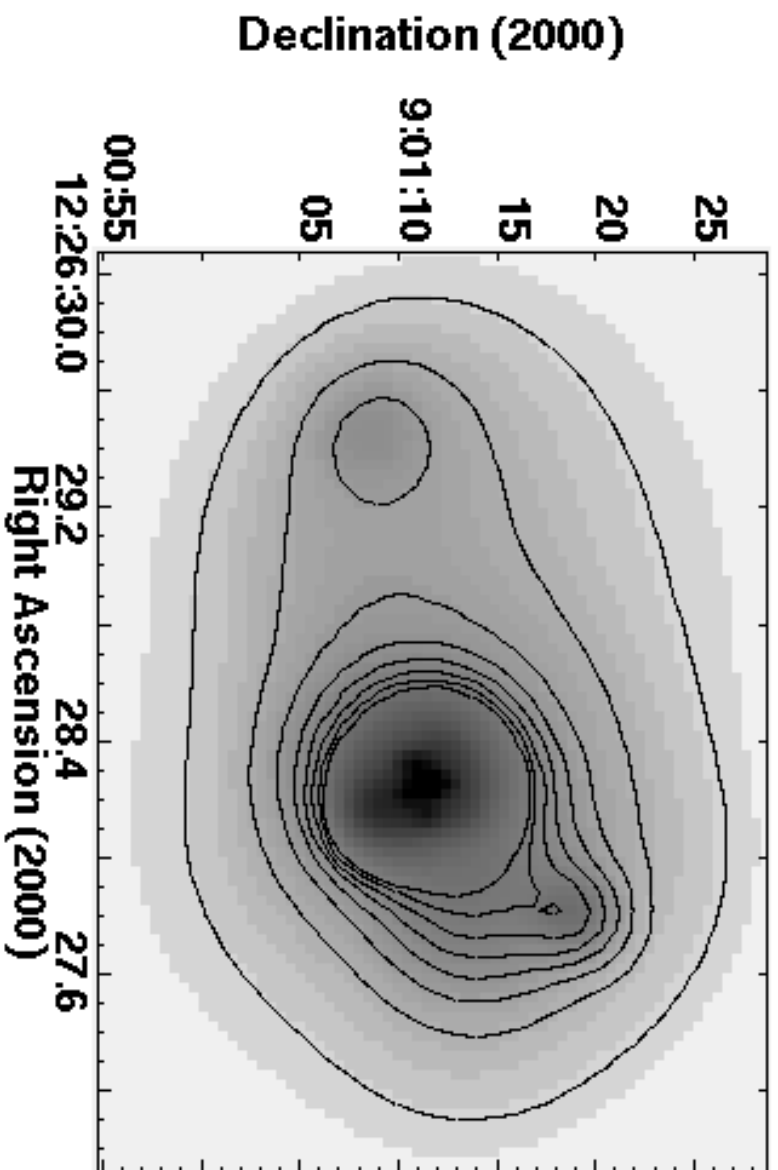
<http://arxiv.org/ps/astro-ph/0307159v1>

This figure "bsmith_fig5.gif" is available in "gif" format from:

<http://arxiv.org/ps/astro-ph/0307159v1>

This figure "bsmith_fig6.gif" is available in "gif" format from:

<http://arxiv.org/ps/astro-ph/0307159v1>

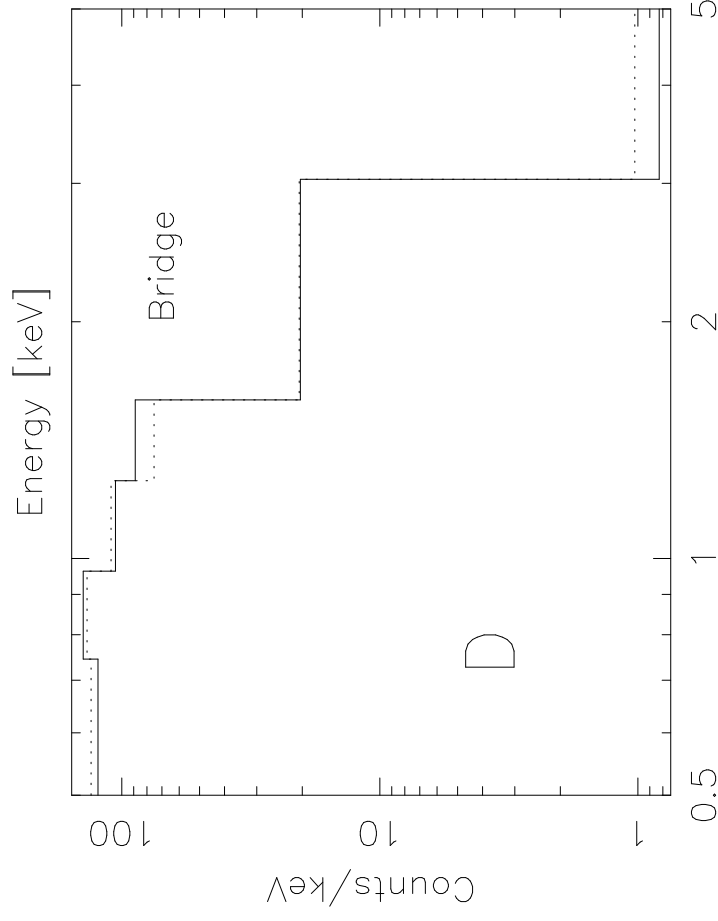
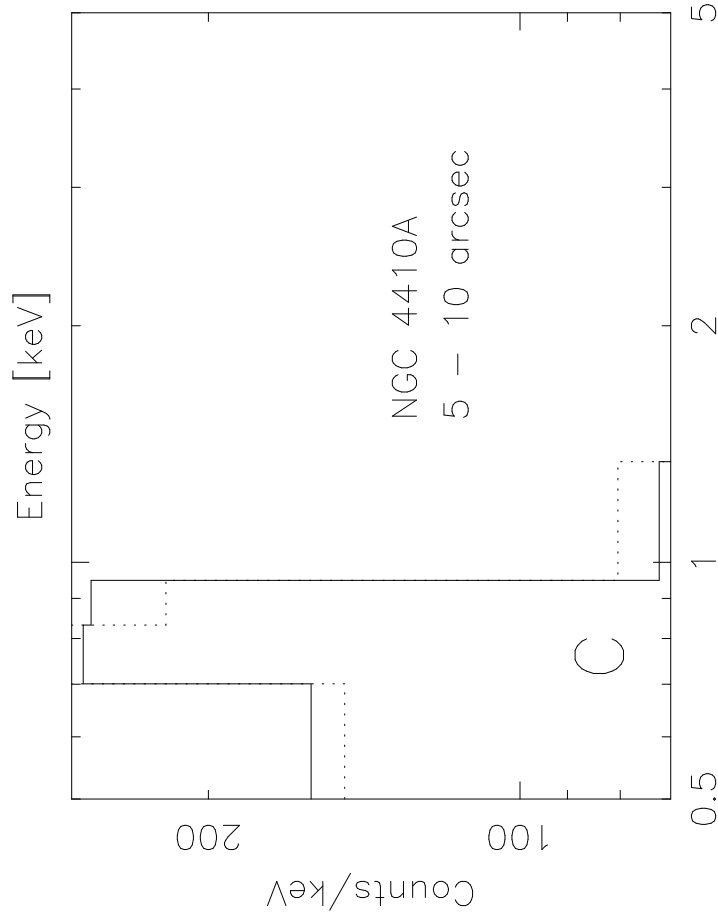
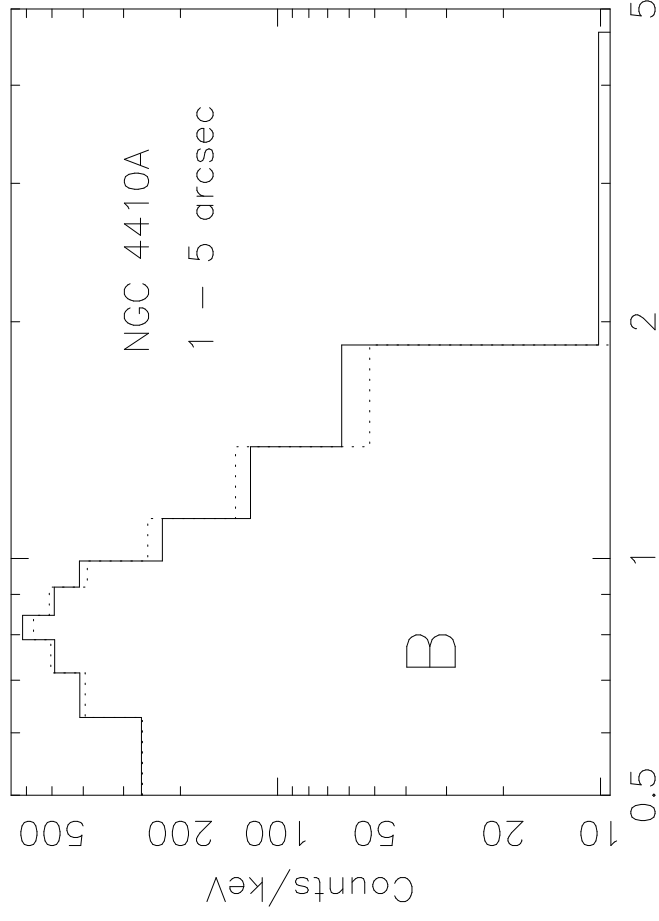
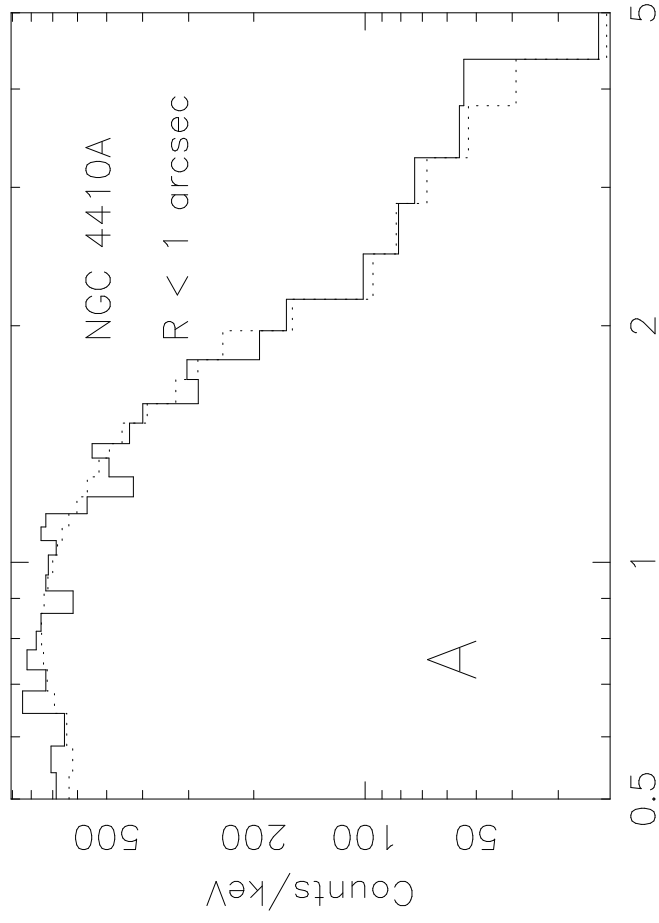


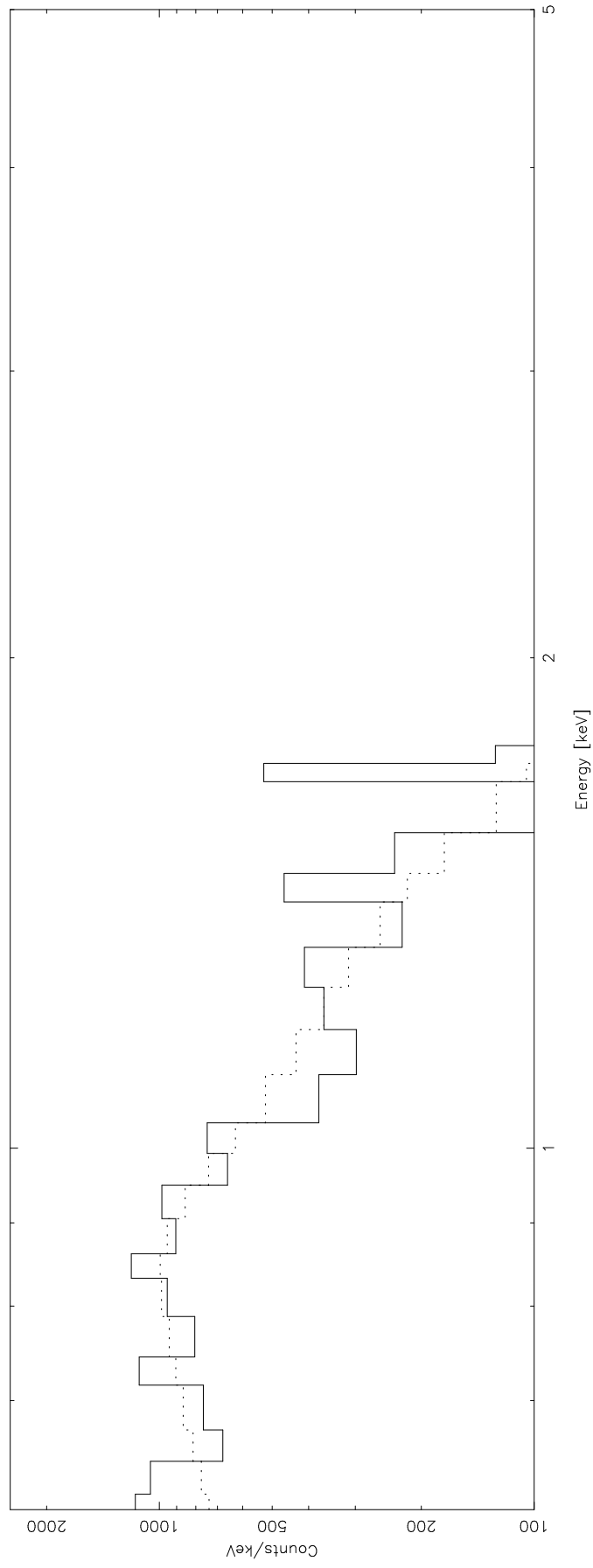
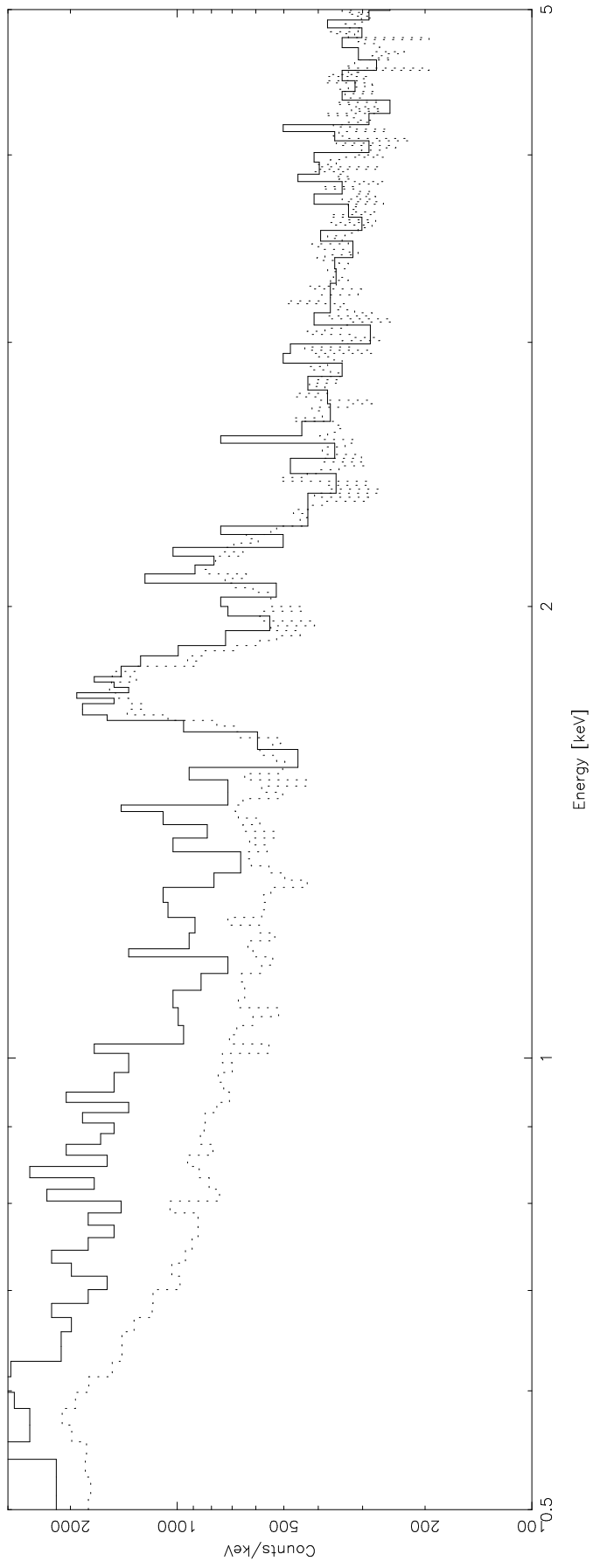
This figure "bsmith_fig9.gif" is available in "gif" format from:

<http://arxiv.org/ps/astro-ph/0307159v1>

This figure "bsmith_fig10.gif" is available in "gif" format from:

<http://arxiv.org/ps/astro-ph/0307159v1>





This figure "bsmith_fig13.gif" is available in "gif" format from:

<http://arxiv.org/ps/astro-ph/0307159v1>